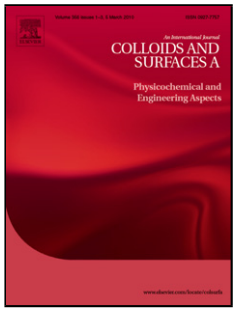

Title: Synthesis and Characterization of Magnetically Separable Ag Nanoparticles Decorated Mesoporous Fe_3O_4@Carbon with Antibacterial and Catalytic Properties

Author: Qian Yu Aiping Fu Hongliang Li Hui Liu Rui Lv Jingquan Liu Peizhi Guo Xiu Song Zhao

PII: S0927-7757(14)00546-9
DOI: http://dx.doi.org/doi:10.1016/j.colsurfa.2014.06.008
Reference: COLSUA 19287

To appear in: *Colloids and Surfaces A: Physicochem. Eng. Aspects*

Received date: 12-4-2014
Revised date: 28-5-2014
Accepted date: 4-6-2014

Please cite this article as: Q. Yu, A. Fu, H. Li, H. Liu, R. Lv, J. Liu, P. Guo, X.S. Zhao, Synthesis and Characterization of Magnetically Separable Ag Nanoparticles Decorated Mesoporous Fe_3O_4@Carbon with Antibacterial and Catalytic Properties, *Colloids and Surfaces A: Physicochemical and Engineering Aspects* (2014), http://dx.doi.org/10.1016/j.colsurfa.2014.06.008

Synthesis and Characterization of Magnetically Separable Ag Nanoparticles Decorated Mesoporous Fe_3O_4@Carbon with Antibacterial and Catalytic Properties

Qian Yu[1], Aiping Fu[1], Hongliang Li[1,*], Hui Liu[1], Rui Lv[2], Jingquan Liu[1], Peizhi Guo[1], Xiu Song Zhao[1,3]

[1] Collaborative Innovation Center for Marine Biomass Fibers, Laboratory of New Fiber Materials and Modern Textile, Growing Basis for State Key Laboratory, College of Chemistry, Chemical Engineering and Environment, Qingdao University, Qingdao 266071, China

[2] Pathogenic Biology Laboratory, Medical College, Qingdao University, Qingdao 266071, China

[3] School of Chemical Engineering, The University of Queensland, St Lucia, Brisbane, QLD 4072, Australia.

Highlights

Porous carbon inlaid with Fe_3O_4 nanoparticles was prepared by a facile approach.

The Fe_3O_4 encapsulated mesoporous carbon was decorated with Ag nanoparticles.

The porous composite matrices showed flexible magnetic separation property.

The Ag nanoparticles decorated porous matrices exhibited catalytic properties.

The Ag nanoparticles decorated matrices possess high antibacterial effect.

Abstract: Mesoporous composite particles of carbon inlaid with Fe_3O_4 nanoparticles (designated as Fe_3O_4@Carbon) with a novel bowl structure and magnetic separation property were fabricated by a spray drying assisted template method using chitosan as carbon precursor and silica nanoparticles as pore directing agent. The influence of the contents among Fe_3O_4 nanoparticles, chitosan and silica nanoparticle on the formation of porous Fe_3O_4@Carbon composite particles has been discussed. Ag nanoparticles were then deposited onto the surface of mesoporous Fe_3O_4@Carbon substrates using silver acetate as precursor with the assistance of ultrasound treatment. The matrices of Ag nanoparticles decorated Fe_3O_4@Carbon composite particles (denoted as Ag-(Fe_3O_4@Carbon)) were

*Corresponding Author, Tel: 0086-532-85950767, E-mail: lhl@qdu.edu.cn

derived and characterized with scanning electron microscopy (SEM), transmission electron microscopy (TEM), X-ray diffraction (XRD) and Fourier-transform infrared (FT-IR) spectroscopy, nitrogen adsorption-desorption, and magnetic property measurements. The Ag-(Fe_3O_4@Carbon) composites showed efficient antibacterial activities to E. coli and S. aureus, high catalytic activity to the reduction of 4-nitrophenol (4-NP) in the presence of $NaBH_4$, strong adsorption ability to organic molecules, and efficient separability under a magnetic field.

Keywords: Mesoporous materials; Ag nanoparticles; Magnetic separation; Antibacterial activity; Catalytic reduction.

1. Introduction

Recently, nanosized Fe_3O_4 (magnetite), as an important member of spinel type ferrite, has shown interesting application potentials in tissue imaging [1], targeted drug delivery [2], environmental area [3], and so on [4,5]. However, the shortcomings of aggregation in suspension, easy oxidation in air and dissolution in an acid medium impede the extensive applications of pristine magnetite nanoparticles [6]. Therefore, a suitable approach to the formation of multifunctional composites consisting of magnetic nanoparticles and other functional components is valuable to avoiding such limitations and improving the physicochemical properties of the nanoparticles [7-9]. Similarly, metallic Ag nanoparticles, which exhibit more efficient antibacterial performance and catalytic properties in comparison with their bulk counterparts, were investigated intensively during the last decade [10-13]. However, due to their high surface energy and high reactivity, Ag nanoparticles are apt to aggregate into large sized agglomerates, resulting in the deterioration of the unique properties of silver. Therefore, dispersion of Ag nanoparticles on a substrate especially a porous one is favorable for a sufficient contact and interaction between Ag and other species. Carbon materials have been regarded as promising candidates for supporting Ag nanoparticles due to their fine chemical durability and high biocompatibility [14-17]. On the other hand, carbon materials have also been intensively exploited as one of the promising matrices for coating or supporting the magnetic nanoparticles owning to its chemical stability, biocompatibility, flexibility of surface modification and pore creation [18-20]. Multifunctional composites possess a novel porous structures and consist of two or more material phases, and therefore their different physicochemical functionalities promise potential applications across vast fields of medicine,

catalysis, adsorption, etc [21-24]. The integration of magnetic nanoparticles and noble metal nanoparticles with a mesoporous matrix can undoubtedly expand the uses of magnetic nanoparticles and noble metal nanoparticles due to the large surface area, tunable porosity and uniform pore size distribution of the porous substrates [25-28]. In return, the integrated nanoparticles of magnetic oxides and noble metal could endow the porous substrates with further desirable functions [7]. Therefore, such novel matrices, which contain multifunctions of porosity, catalysis, antibacterial activity, magnetic separation, etc., have attracted high attention in adsorption [29], biomedicine [30], drug delivery targeting [31], and chemical engineering [32]. Unfortunately, the synthesis of these desirable multifunctional structures generally requires complicated multiple steps and involves organic solvents or high temperatures[33-35], limiting the mass production of these promising matrices.

In this paper, we reported on a facile and mass-producible approach for the preparation of multifunctional matrices, namely Ag nanoparticles decorated porous Fe_3O_4@Carbon (denoted by Ag-(Fe_3O_4@Carbon)). Intermedia of SiO_2 and Fe_3O_4 nanoparticles co-encapsulated chitosan particles called as (SiO_2, Fe_3O_4)@Chitosan were firstly synthesized by a spray drying assisted template method, in which chitosan and commercial colloidal SiO_2 nanoparticle were designed as carbon precursor and pore directing templates, respectively. After the carbonization of the intermedia (SiO_2, Fe_3O_4)@Chitosan particles and the subsequently etching of the silica nanoparticle templates, porous carbon particles inlaid with magnetic Fe_3O_4 nanoparticles (denoted by Fe_3O_4@Carbon) were obtained. The optimal contents of Fe_3O_4 particles, chitosan, and colloidal silica were deduced based on the morphology studies and nitrogen sorption measurements of the Fe_3O_4@Carbon products. Then Ag nanoparticles were deposited onto the surface of the porous Fe_3O_4@Carbon substrates using ethanol/water solution of silver acetate as precursor. As a result, multifunctional matrices involving Fe_3O_4 nanoparticles encapsulated porous carbon composite substrates (Fe_3O_4@Carbon) which were decorated with Ag nanoparticles were achieved successfully (Ag-(Fe_3O_4@Carbon)). Herein, ultrasound treatment and mechanical stirring were applied to the conversion of Ag^+ ions to metallic Ag nanoparticles, and both of the approaches can result in the Ag-(Fe_3O_4@Carbon) matrices. Nevertheless, the ultrasound treatment was considered as the preferred strategy for the reduction of Ag^+ based on the analysis of morphology and crystallinity of the resultant Ag nanoparticles. Finally, adsorption, magnetic separation property,

antibacterial activity and catalytic property of the multifunctional matrices were investigated in detail.

2. Experimental Section

2.1. Materials

Colloidal silica (GRACE LUDOX, AS-40, 40%, ~12 nm, U.S.A), chitosan (degree of deacetylation 90%), ferric chloride hexahydrate ($FeCl_3 \cdot 6H_2O$), ethylene glycol (EG), polyethylene glycol (PEG, 4000), sodium acetate trihydrate ($NaAc \cdot 3H_2O$), sodium hydroxide (NaOH), silver acetate (AgAc), sodium borohydride ($NaBH_4$) and 4-nitrophenol (4-NP) were of analytical grade and used as received without further purification. Distilled water was used in the experiments.

2.2. Synthesis of Fe_3O_4 nanoparticles

The fabrication of Fe_3O_4 nanoparticles was achieved through a modified polyol-medium solvothermal method reported by Li et al. [36]. 1.35 g of $FeCl_3 \cdot 6H_2O$ was dissolved in 40 mL of ethylene glycol under magnetic stirring, forming a transparent yellow solution. Then 1.0 g of polyethylene glycol 4000 and 3.6 g of $NaAc \cdot 3H_2O$ were dissolved in the above solution. The resultant mixture was then transferred into a Teflon lined autoclave and heated at 200℃ for 8 h. After that, black products were collected with the assistance of an external magnetic field, and then rinsed twice with deionized water and ethanol. Finally, the products were dried in vacuum at 50℃ for further applications.

2.3. Synthesis of mesoporous magnetic Fe_3O_4@Carbon (FC) composite particles

SiO_2 and Fe_3O_4 nanoparticles co-encapsulated chitosan intermedia microspheres were firstly obtained using a laboratory-scale SP-1500 spray dryer (ShangHai SunYi tech CO., LTD.) by the following procedure. Given amounts of silica colloid and 2 wt% aqueous solution of chitosan dissolved in 5 wt% diluted acetic acid were mixed and then kept stirring constantly until them turned into a homogeneous suspension. Another suspension of Fe_3O_4 nanoparticles in distilled water was prepared under the treatment of ultrasound for 30 min and then was mixed with the above suspension. After a mechanical stirring for 2 h, the liquid mixture was then sprayed into the chamber of a laboratory-scale spray dryer at 160℃ using pressurized air as carrier gas, and the dried particles were automatically collected by an integrated cyclone separator. The resultant intermedia particles denoted by (SiO_2, Fe_3O_4)@chitosan were then carbonized in a programmed tube furnace under nitrogen atmosphere. The temperature was raised to 500℃ at a heating rate of 2

℃ per minute and kept at this temperature for 5 h, then cooled down to room temperature naturally. Subsequently, the obtained powder was dispersed into a 1 mol/L aqueous solution of NaOH at 50℃ for 24 h under stirring to etch away the silica nanoparticles. After washing three times with water and a freeze-drying process on a FD-1A-50 freeze-dryer, black powders of mesoporous carbon inlaid with Fe_3O_4 nanoparticles were then generated. The resultant sample was denoted by Fe_3O_4@Carbon and abbreviated to FC. Scheme 1 schematically illustrates the synthetic process of the porous substrate.

Mesoporous Fe_3O_4@Carbon particles derived from the same dosages of Fe_3O_4 nanoparticles (0.1 g) and chitosan (0.375 g) mixed with different amounts of colloidal silica of 3 and 1.5 mL were designated as FC-1 and FC-2, respectively. The sample made from 0.05 g of Fe_3O_4 and 0.375 g of chitosan mixed with 1.5 mL of colloidal silica was denoted as FC-3.

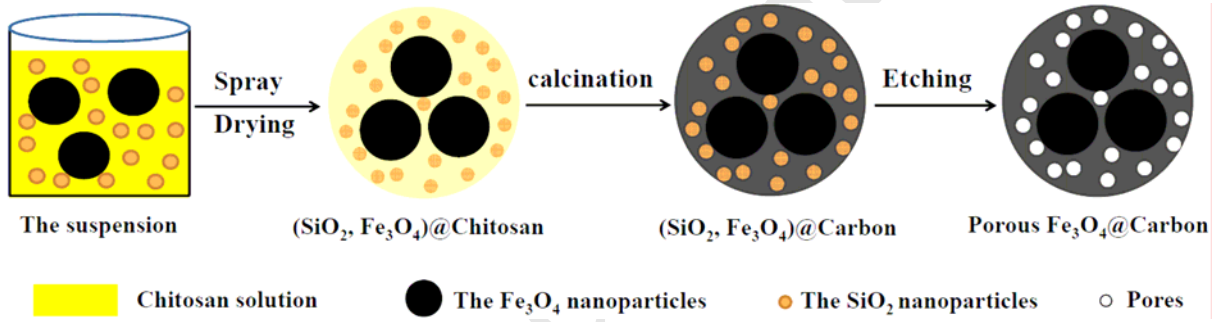

Scheme 1. Formation process of the porous Fe_3O_4@Carbon composite particles (FC).

2.4. Synthesis of Ag nanoparticles decorated Fe_3O_4@Carbon composites (Ag-FC)

0.1 g of mesoporous Fe_3O_4@Carbon particles were dispersed into 20 mL water/ethanol (1/1, V/V) solution of silver acetate (0.1 g). The suspension was then irradiated with high intensity ultrasound for 2 hours. After the treatment, solids in the suspension were collected by centrifugation, and then dried with a thermostatic oven at 50℃. The sample derived from the ultrasound treatment was designated as Ag-(Fe_3O_4@Carbon)-U and was abbreviated to Ag-FC-U. As control experiment, the suspension of mesoporous Fe_3O_4@Carbon particles dispersed in water/ethanol (1/1, V/V) solution of silver acetate was also subjected to mechanical stirring for 2 h at ambient temperature of about 20℃. Sample, named as Ag-FC-M, was obtained with the similar separation and drying process as used for Ag-FC-U.

2.5. Adsorption and magnetic separation

Adsorption and magnetic separation abilities of the Ag-(Fe_3O_4@Carbon) samples were investigated using methylene blue (MB) as a model adsorbate. A given amount of

Ag-(Fe_3O_4@Carbon) samples (5mg) were dispersed into an aqueous solution of methylene blue with a concentration of about 25 mg/L. After an treatment with ultrasound for about 10s, the suspension was placed close to a magnet for separation.

2.6. Catalytic reduction of 4-nitrophenol

The catalytic reduction of 4-NP was carried out in a standard quartz cuvette and the process was monitored by a UV-Vis spectrophotometer to examine the catalytic activity of the synthesized Ag-(Fe_3O_4@Carbon) matrix in the presence of an excess amount of $NaBH_4$. The reaction procedure was as follows: 2.0 mL of deionized water, 0.1 mL of 4-NP solution (0.005 mol/L), and 1.0 mL of freshly prepared $NaBH_4$ aqueous solution (0.2 mol/L) were added into a quartz cuvette. Then the color of the solution turned to bright yellow immediately. At this stage, the nitrophenol was converted to nitrophenolate anion. Subsequently, 5 mg of Ag-(Fe_3O_4@Carbon) catalyst was added to the solution and stirred thoroughly, and the mixture was then monitored by measuring the adsorption at λ_{max} = 400 nm every 2 min using a UV-Vis spectrophotometer. As the reaction proceeded, the peak at λ_{max} = 400 nm corresponding to the p-nitrophenolate ion disappeared due to its conversion to p-aminophenolate ions with time and the solution changed gradually from bright yellow to transparent. As control experiment, similar reaction has also been performed using porous Fe_3O_4@Carbon particles instead of Ag-(Fe_3O_4@Carbon) as catalyst.

2.7. Measurements of the antibacterial activity

E. coli (ATCC25922) and S. aureus (ATCC6538), which have been chosen as representative bacteria for the Gram-negative bacteria and Gram-positive bacteria, respectively, were used to test the antibacterial activity of the Ag-(Fe_3O_4@Carbon) composites. The tests were performed as follows [37]: all glassware and materials were sterilized by autoclaving at 120℃ for 15 min before the microbiological experimentation. Then 0.1g of the Ag-(Fe_3O_4@Carbon) sample was dispersed into a conical flask containing 47.5 ml of PBS (phosphate-buffered saline) solution and 2.5 ml of nutrient broth inoculated by 10^5 cfu (colony forming units)/ml of E. coli or S. aureus. The suspension were then kept shaking at 37℃ in a water-bathing constant temperature oscillator for 4 h. After that, 0.5 ml of the mixture was dispersed into the nutrient agar plate and incubated at 37℃ overnight. To study further on the antibacterial effects of the composite, the minimum inhibitory concentrations (MICs) were detected with broth by the usual twofold serial dilution method [38]. Suspensions of Ag-(Fe_3O_4@Carbon) particles dispersed into the broth at different concentrations

were obtained by twofold serial diluting its initial suspension (625 μg/mL), and then the serial of twofold diluted suspensions were sterilized by autoclaving. After inoculating with E. coli or S. aureus, respectively, the diluted suspensions were incubated at 37 ˚C overnight and then examined by monitoring their turbidity without shaking. Similar test, as control experiment, has also been performed with the porous Fe_3O_4@Carbon particles.

2.8. Characterization

The morphologies and the structures of the samples were examined by a JEOL JSM-6390LV scanning electron microscope (SEM) and a JEM-2010F transmission electron microscope (TEM). Fourier transformation infrared (FTIR) spectra were recorded with a Nicolet 5700 FTIR spectrometer on KBr pellets. A TAS-986 flame atomic absorption spectrophotometer (FAAS) was used for the detection of the silver loading contents by dissolving the Ag nanoparticles with dilutes aqueous solution of nitric acid. The specific surface areas were estimated using the Brunauer-Emmett-Teller (BET) method with a TriStar 3000 Surface Area and Pore Analyzer (Micromeritics). Powder X-ray diffraction (XRD) patterns were collected using a Bruker D8 advance X-ray diffractometer equipped with graphite monochromatized Cu Kα radiation (λ=0.15418 nm). UV-Vis spectra were measured through a TU-1901 UV-Visible spectrophotometer (Purkinje General). Magnetic properties of the composites were characterized using a superconducting quantum interference device (SQUID) magnetometer with fields of up to ±1.5T.

3. Results and Discussion

3.1. FTIR Spectra

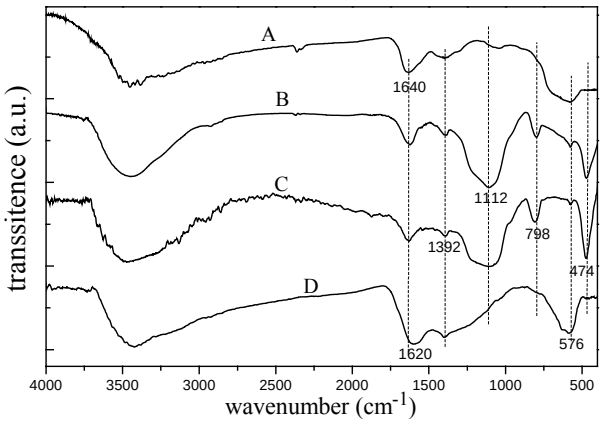

Fig. 1 FT-IR spectra of (A) Fe_3O_4, (B) (SiO_2, Fe_3O_4)@Chitosan, (C) (SiO_2, Fe_3O_4)@Carbon, and (D) porous Fe_3O_4@Carbon.

Fig. 1 shows the FT-IR spectra of pristine Fe_3O_4 nanoparticles (curve A), (SiO_2, Fe_3O_4)@Chitosan intermedia particles (curve B), (SiO_2, Fe_3O_4)@Carbon particles (curve C) and porous Fe_3O_4@Carbon particles (curve D). The characteristic peaks of Fe_3O_4 at 576 cm^{-1} can be observed in all of the four curves, indicating that the Fe_3O_4 nanoparticles were preserved after the spray drying process and the etching treatment. The broad peak around 3500 cm^{-1} was ascribed to the adsorbed water in the samples. In curve B, the characteristic peaks of chitosan could be observed, for instance, the band of 1620 cm^{-1} was assigned to the N–H bending vibration and the peak at 1392 cm^{-1} to a –C–O stretching of the primary alcoholic group in chitosan [39]. The characteristic peaks of silica, which was assigned to the asymmetric stretching vibration of Si-O-Si, could be observed at 1112 cm^{-1} in curves B and C. While, the peaks at 798 and 474 cm^{-1} correspond to the symmetric stretching vibration and the bending vibration of Si-O-Si [40]. By contrast, the bands at 1112, 798 and 474 cm^{-1} corresponding to the vibration of Si-O-Si disappeared in curve D, confirming that the embodied SiO_2 nanoparticles have been completely removed after the etching process by NaOH aqueous solution.

3.2. SEM and TEM studies

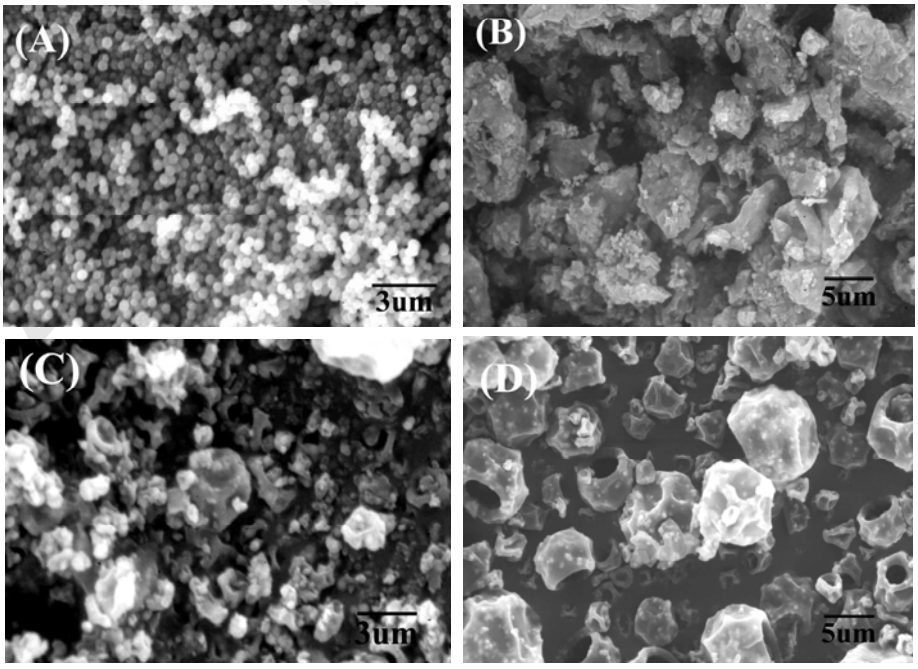

Fig. 2 SEM images of (A) Fe_3O_4 microspheres, (B) FC-1, (C) FC-2 and (D) FC-3.

The SEM image of Fe_3O_4 nanoparticles, which was used as magnetic cores in the preparation of the Fe_3O_4@Carbon composite particles, is shown in Fig. 2A. The Fe_3O_4 particles showed spherical morphology with an average size of about 250 nm. Images B, C and D in Fig. 2 present the images of the Fe_3O_4@Carbon composites prepared with different contents of Fe_3O_4 nanoparticles, chitosan and colloidal silica corresponding to 0.1g: 0.375g: 3mL, 0.1g: 0.375g: 1.5mL and 0.05g: 0.375g: 1.5mL, respectively. In comparison with the rough surface of FC-1 (Fig. 2B), sample FC-2 (Fig. 2C), which was fabricated with the same amounts of Fe_3O_4 and chitosan as FC-1 (0.1g and 0.375g) while the volume of colloidal silica was halved, showed a smooth surface but irregular morphology. With the reduction of the content of Fe_3O_4 nanoparticles from 0.1 to 0.05 g, while maintaining the amounts of chitosan (0.375g) and colloidal silica (1.5mL) constant, the Fe_3O_4@Carbon composite particles with a more homogenous size distribution were obtained (see images C and D). Moreover, a novel bowl-like shape was formed in the latter two cases. The difference among FC-1, FC-2 and FC-3 might arise from the influences of the colloidal silica and the Fe_3O_4 nanoparticles on the solidification of the suspension droplets during the spray drying process. The silica nanoparticles were used as sacrificial templates for directing the pores, therefore, the morphology of samples prepared with more silica particles might be distorted after the etching of the silica particles with NaOH aqueous solution. As a result, more irregular particles were observed in Fig. 2C than in Fig 2B. The Fe_3O_4 nanoparticles were utilized as magnetic cores for Fe_3O_4@Carbon composite particles. It can also be seen that with the reduction of the content of Fe_3O_4 nanoparticles, porous Fe_3O_4@Carbon composite particles with an average size of about 5 μm and a more homogenous size distribution were acquired (see images C and D). A more detailed structure of FC-3 was probed by TEM measurement (see the following section).

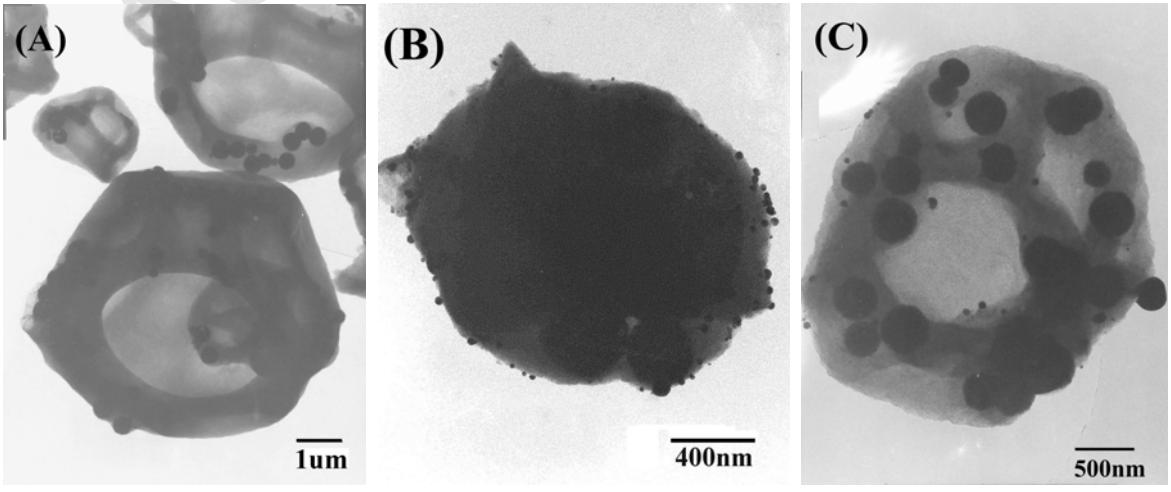

Fig. 3 TEM images of (A) FC-3, (B) Ag-FC-U and (C) Ag-FC-M.

Fig. 3 shows the TEM images of FC-3 composite particles (image A), and the corresponding Ag decorated porous Fe_3O_4@Carbon matrices (image B, Ag-FC-U; image C, Ag-FC-M), respectively. It can be seen that Fe_3O_4 nanoparticles were successfully embedded in the matrix of carbon, and the bowl-shaped structure was clearly visible. Considering that the bowl structure can improve its physical and chemical properties, especially the specific surface area (refer to Fig. 6), we chose FC-3 sample for the subsequent silver nanoparticles decoration. One typical TEM image of the Ag-FC-U particle is shown in Fig. 3B, and from the image one can see clearly that Ag nanoparticles with size in range of 20-50 nm were anchored on surface of the Fe_3O_4@Carbon substrate after the ultrasound treatment of silver acetate ethanol/water solution (the formation of metallic Ag, please refer to XRD analysis). The loading ratio of Ag nanoparticles detected by FAAS was about 24 wt%. Fig. 3C showed that several small silver nanoparticles can also be loaded onto the surface of the Fe_3O_4@carbon particles by a simple stirring method, but the loading ratio of silver nanoparticles is only about 13 wt%, which is lower than that on the sample obtained by ultrasound assisted loading process (this speculation was supported further by the XRD studies, see the following section).

3.3. XRD Analysis

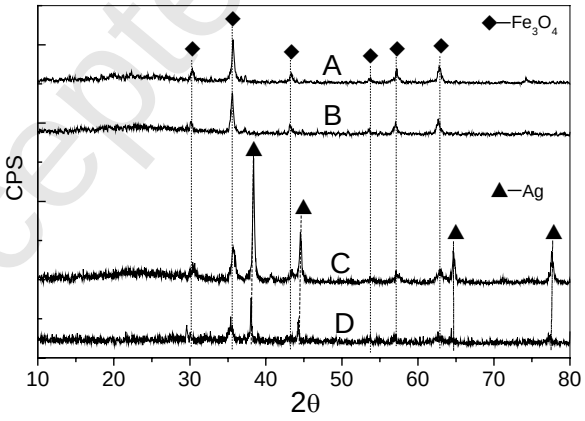

Fig. 4 XRD patterns of the Fe_3O_4 nanoparticles (curve A), the porous Fe_3O_4@Carbon particles (curve B), and those of the Ag nanoparticles decorated Fe_3O_4@Carbon composite particles (curve C, Ag-FC-U and curve D, Ag-FC-M).

Fig. 4 shows the representative XRD patterns of the pristine Fe_3O_4 nanoparticles (curve A), the Fe_3O_4@Carbon particles (curve B), and the Ag nanoparticles decorated Fe_3O_4@Carbon composite matrices of Ag-FC-U (curve C) and Ag-FC-M (curve D), respectively. A series of characteristic

peaks at 2θ = 30.2, 35.5, 43.1, 53.4, 57.0, and 62.6 were observed in all of the four curves. These diffraction peaks match well in position and intensity with the standard XRD date of Fe_3O_4 with a cubic inverse spinel structure (JCPDS No. 19-0629). No peaks of other iron oxide phases were observed in these XRD patterns, and it can be attributed to the protection effect of the carbon layer which prevented the magnetic core from oxidizing [7, 41]. The characteristic diffraction peaks of the Fe_3O_4 nanoparticles in the Ag-(Fe_3O_4@Carbon) matrices did not differ from that of the pristine Fe_3O_4 nanoparticles and the Fe_3O_4@Carbon sample, indicating that the Ag loading procedure did not influence the crystal structure of the Fe_3O_4 nanoparticles. Besides the characteristic peaks of Fe_3O_4, additional intense diffraction peaks at 2θ = 38, 44, 65 and 77 were observed in the XRD curves of these two Ag-(Fe_3O_4@Carbon) matrices of Ag-FC-U and Ag-FC-M, which can be indexed to the (1 1 1), (2 0 0), (2 2 0) and (3 1 1) planes of cubic metallic Ag (JCPDS No. 04-0783). Ultrasound has been proven to be a kind of powerful technique for promoting the reduction of Ag^+ to Ag since the high intensity ultrasound can cleave the solvent molecules and induce radicals, which then can act as the reductive agent [42,43]. Unexpectedly, a part of the Ag^+ ions were also reduced to metallic Ag during the mechanical stirring process. It can be explained as due to the existence of active groups, such as the residual C-NH_2, C-OH and C-H groups, on the surface of the Fe_3O_4@carbon particles, which played the role in the reduction of Ag^+ [44]. Obviously, the peak intensity of metallic Ag in Ag-FC-M was much weaker than that in sample Ag-FA-U, demonstrating that less metallic Ag nanoparticles were formed upon just a simple mechanical stirring process. All in all, the XRD result is consistent with the TEM observation.

3.4. Nitrogen adsorption-desorption measurements

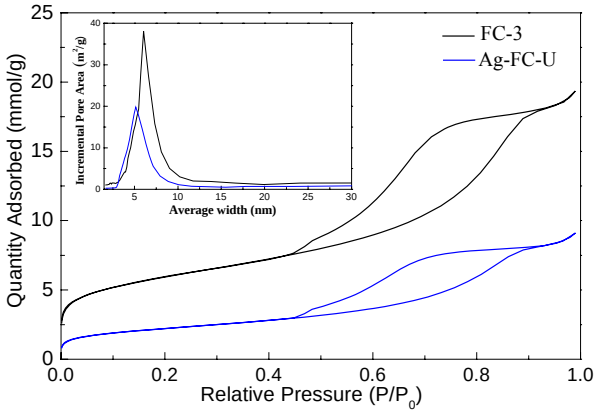

Fig. 5 Nitrogen adsorption-desorption isotherms and the corresponding pore-size distributions (the inset) of FC-3 and Ag-FC-U.

N_2 adsorption-desorption measurements were carried out to determine the specific surface area and pore size distributions of Fe_3O_4@Carbon and Ag-(Fe_3O_4@Carbon) composites. The isotherms and corresponding pore size distributions are shown in Fig. 5. Both the samples contain hysteresis loops which can be classified as type IV isotherm characteristic of porous structures [45, 46]. The isotherms of FC-3 particles and Ag-FC-U composite matrix were calculated via the Barret-Joyner-Halenda (BJH) method. As a result, BET surface area, pore volume and pore size distribution of 521 m^2g^{-1}, 0.6 m^3g^{-1} and 6.1 nm for the former, and 178 m^2g^{-1}, 0.3 m^3g^{-1} and 5.0 nm for the latter were deduced from the calculations. Such a large specific surface area of FC-3 arose mainly from the pores within the matrix generated by removing the templates of silica nanoparticles and also possibly resulted from its external surfaces of the bowl-shaped structure. In comparison with FC-3, the Ag-FC-U matrix showed a lower specific surface area and a smaller pore volume. This can be attributed to the loading of Ag nanoparticles into the pores, especially the large sized ones, of the porous Fe_3O_4@Carbon substrates [42].

3.5. Magnetic and adsorption properties

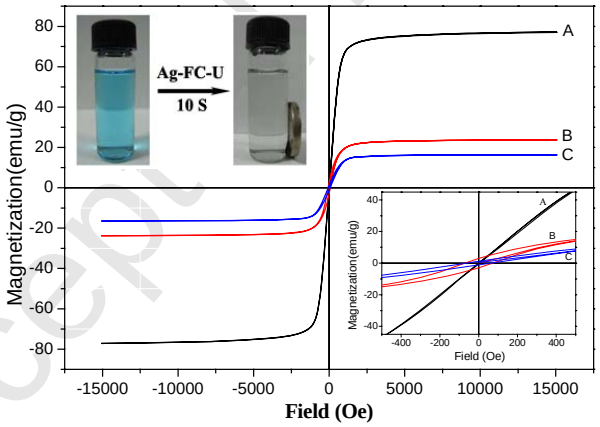

Fig. 6 Room-temperature magnetic hysteresis loops of (A) Fe_3O_4, (B) Fe_3O_4@Carbon, (C) Ag-(Fe_3O_4@Carbon). The bottom inset is a magnification of the magnetic hysteresis loops. The upper inset is a photograph of the adsorption of MB by Ag-(Fe_3O_4@Carbon) and their response to an external magnet.

The room-temperature magnetic hysteresis loops of different samples are shown in Fig. 6. The values of saturation magnetization for pristine Fe_3O_4 nanoparticles, Fe_3O_4@Carbon (FC-3) particles and Ag-(Fe_3O_4@Carbon) (Ag-FC-U) matrices were 77.41, 23.49 and 15.96 emu/g, respectively. The saturation magnetizations of Fe_3O_4@Carbon and Ag-(Fe_3O_4@Carbon) are lower than that of pristine Fe_3O_4 nanoparticles, which can be ascribed to the existence of nonmagnetic carbon and Ag

in the total mass. Very low coercivity or remanence could be observed for the pristine Fe_3O_4 nanoparticles, suggesting their superparamagnetic properties [47]. Whereas the samples of Fe_3O_4@Carbon and Ag-(Fe_3O_4@Carbon) showed obvious coercivity with values of about 68 and 50 Oe, respectively, indicating their weak ferromagnetic behavior (as shown in the bottom inset of Fig. 6). The slight changes of coercivity for the Fe_3O_4 nanoparticles in different matrices might be attributed to the influence of the surrounding environment [7,41,48]. The adsorption experiment revealed that the Ag-(Fe_3O_4@Carbon) matrix owns a strong and fast adsorption to methylene blue, and thereafter can respond rapidly to an external magnetic field (see the upper inset). These results suggest that the porous Ag-(Fe_3O_4@Carbon) composite particles possess excellent adsorption ability to organic species and strong magnetic response to an external magnetic field.

3.6. Catalytic reduction of p-nitrophenol

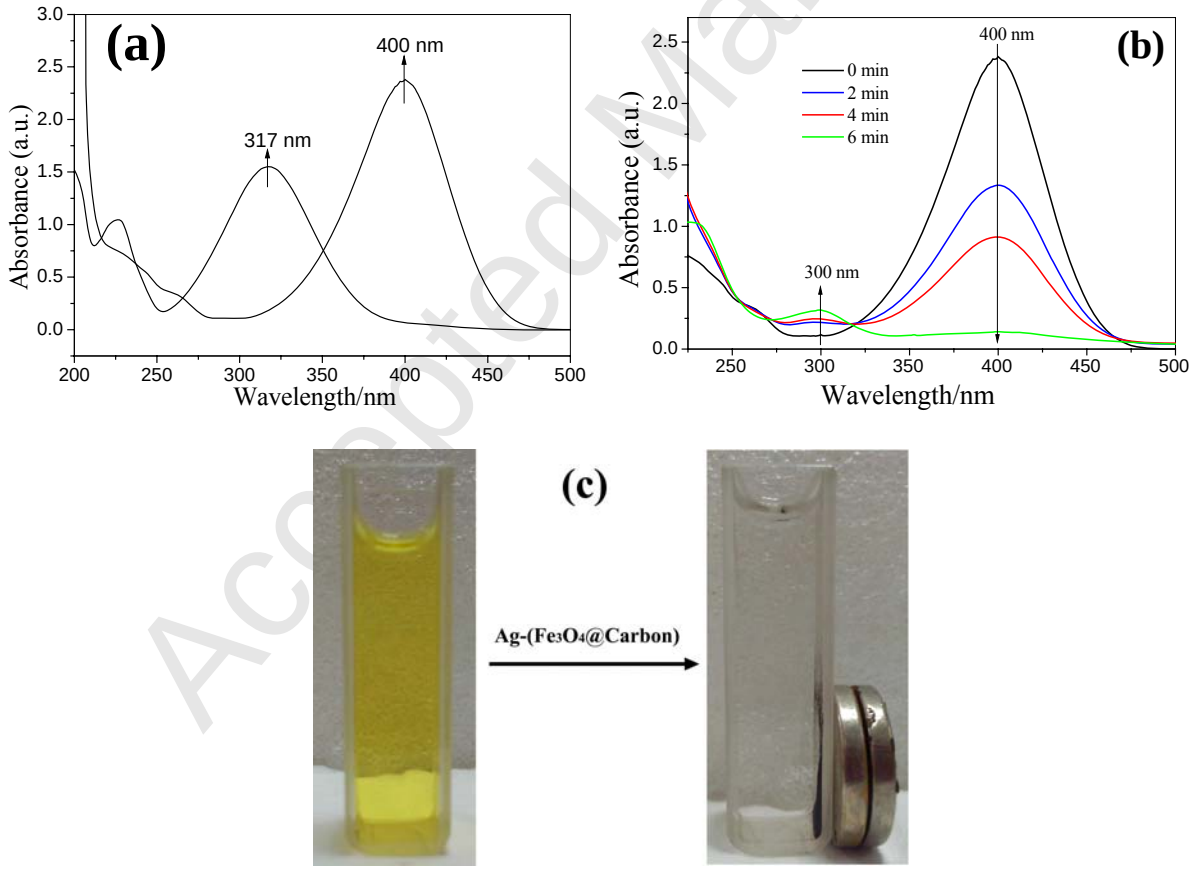

Fig. 7 UV-Vis spectra of 4-NP in the absence or presence of $NaBH_4$ (a); Time dependent UV-Vis spectra for the catalytic reduction of 4-NP using Ag-(Fe_3O_4@Carbon) (Ag-FC-U) as a catalyst (b); and Photographs of the reduction of 4-NP by $NaBH_4$ in the presence of Ag-(Fe_3O_4@Carbon) and the magnetic separation of the catalyst after the catalytic reaction (c).

The catalytic activity of Ag-(Fe_3O_4@Carbon) composites were substantiated through p-nitrophenol reduction to its sole product of p-aminophenol (4-AP) in the presence of $NaBH_4$ as a reductant [49,50]. The extent of catalytic reaction can be followed by measuring the change of light absorbance of the solution at 400 nm and 300 nm (see panel (b) of Fig. 7) [51,52]. As has been shown in Fig. 7a, the absorption peak at 317 nm corresponding to the pure 4-NP shifted to 400 nm after the addition of the freshly prepared $NaBH_4$ solution, and the color of the solution changed also from light yellow to bright yellow, indicating the formation of 4-nitorphenolate ions in an alkaline condition. The bright yellow solution was very stable and the absorption kept unchanging even after adding excess $NaBH_4$ solution for more than 2h, which confirmed that the reduction did not proceed in the presence of only $NaBH_4$ solution. In contrast, the catalytic activity of Ag-(Fe_3O_4@Carbon) toward 4-NP reduction is convincingly demonstrated by the time-dependent UV-Vis absorption spectra recorded every 2 min as shown in Fig. 7(b). With the introduction of Ag-(Fe_3O_4@Carbon) catalyst into the reaction solution, the absorption peak at 400 nm successively decreased within 6 min and a new peak at 300 nm increased gradually. The new absorption at 300 nm is the characteristic peak of p-aminophenol [53], and its appearance thereafter indicated the reduction of 4-NP to 4-AP. Due to the strong adsorbing ability of the porous Ag-(Fe_3O_4@Carbon) catalyst, $NaBH_4$ and 4-NP could be rapidly concentrated into the pores of the porous composite catalysts, where the Ag nanoparticles could relay electrons from the donor of BH_4^- to the acceptor of 4-NP to promote the occurrence of reduction [54]. It can be seen from Fig. 7 (c) when the porous composite catalyst was added to the solution, the bright yellow solution changed gradually to colorless. The catalyst can be easily separated after the catalytic reduction upon the contact with a magnet and the recycled Ag-(Fe_3O_4@Carbon) can then be reused. These results confirmed that the Ag-(Fe_3O_4@Carbon) composites are effective catalyst for the reduction of p-nitrophenol and own magnetic response to be conveniently separated and recycled. However, control experiment showed that Fe_3O_4@Carbon substrates without Ag nanoparticles can not promote the reduction of 4-NP to 4-AP by $NaBH_4$, confirming the role of metallic Ag nanoparticles in the reduction process.

3.7. Antibacterial properties

Four plates containing the same content of bacteria and nutrient agar were used for the antibacterial tests, and the results are presented in Fig. 8. The differences among them are that plates A and C include Fe_3O_4@Carbon particles, which were designed as control samples, while

plates B and D involve Ag-(Fe_3O_4@Carbon) composites. In plates B and D, there was almost no bacteria growth in the medium, indicating Ag-(Fe_3O_4@Carbon) composites exhibited remarkable antibacterial activity. Whereas, the control groups (A and C) contained porous Fe_3O_4@Carbon particles showed several obvious colonies of bacteria, revealing that the porous FC particles have no antibacterial activity. Therefore, we can conclude that the antibacterial activity of Ag-(Fe_3O_4@Carbon) was attributed to the existence of the Ag nanoparticles. The porous structure of the Ag-(Fe_3O_4@Carbon) particles could promote sorption of the bacteria onto their surface due to their large surface area, which increased the chance for the antimicrobial metallic Ag nanoparticles to contact with the bacteria and then damaged and altered their functionality [14, 55].

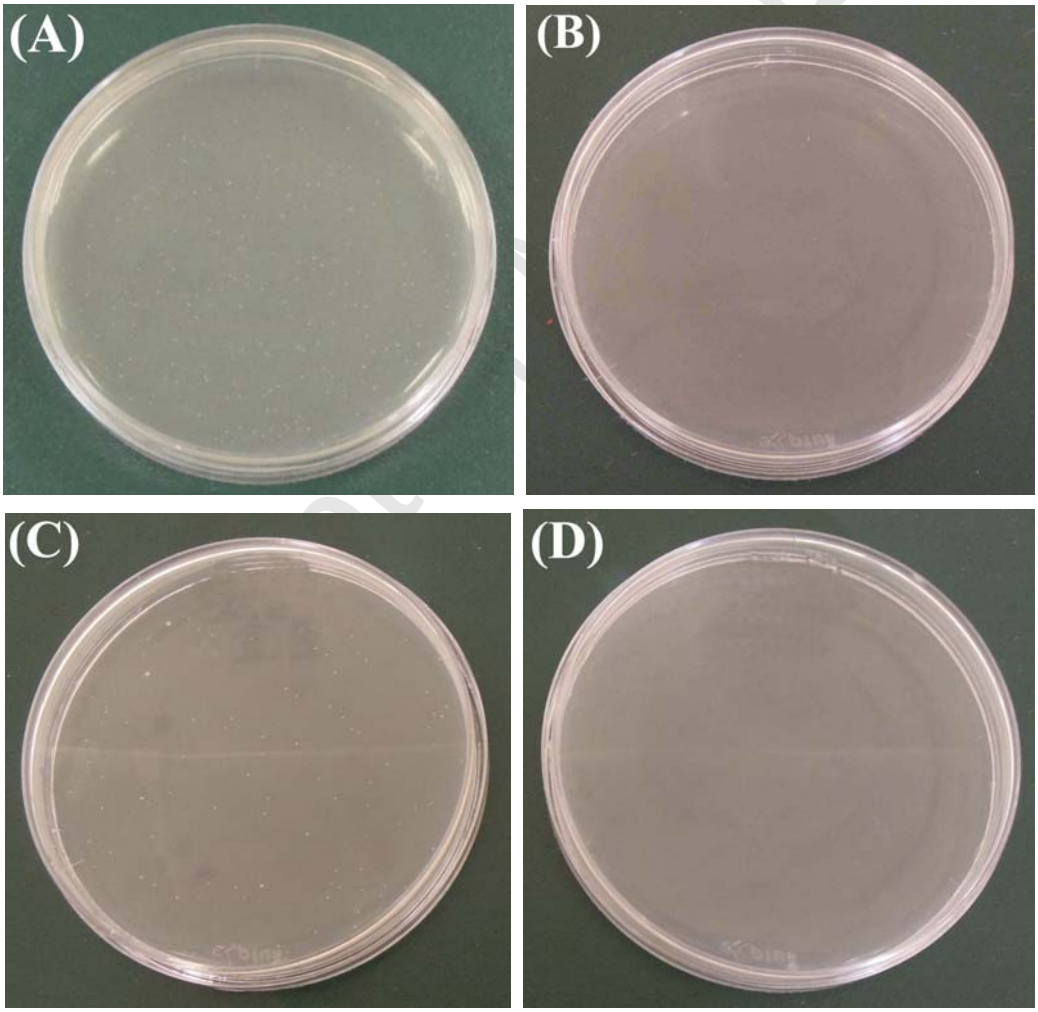

Fig. 8 Photographs of the antibacterial test results for FC-3 (A, C) and Ag-FC-U (B, D) against E. coli (A, B) and S. aureus (C, D).

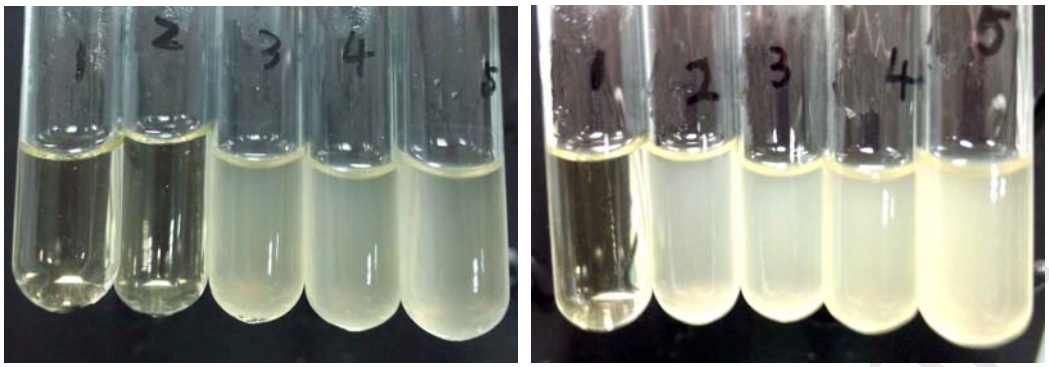

Fig. 9 Photographs of the tubes used for determining the minimum inhibitory concentrations of Ag-FC-U composites against E. coli (left) and S. aureus (right).

To obtain the minimum inhibitory concentrations (MIC) of Ag-FC-U against E. coli and S. aureus, the test systems with different dosages of the Ag-(Fe_3O_4@Carbon) particles were investigated and the photographs of them were presented in Fig. 9. MIC values of 156 μg/mL to E. coli and 312 μg/mL to S. aureus, respectively, for the Ag-FC-U composites have been deduced. The differences of the MIC values of Ag-(Fe_3O_4@Carbon) to E. coli and to S. aureus can be ascribed to the antibacterial selectivity of the metallic Ag nanoparticles [56].

4. Conclusions

The spray drying assisted template method combined with calcinations is an efficient approach for preparation of the Fe_3O_4 nanoparticles encapsulated porous carbon substrates (Fe_3O_4@Carbon). The silica nanoparticles played the role in directing pores in the Fe_3O_4@Carbon composite particles and they can be easily removed by etching with aqueous solution of NaOH. The morphology of the Fe_3O_4@Carbon particles can be modified by adjusting the contents of the precursors. A preferred content of about 0.05g: 0.375g: 1.5ml among the Fe_3O_4 nanoparticles, colloidal silica and chitosan precursors was derived for producing the Fe_3O_4@Carbon particles with a novel bowl-shaped structure. The porous Fe_3O_4@Carbon substrates showed a specific surface area up to 500 m^2g^{-1}, and the high specific surface area improved greatly their ability to the adsorption of organic species as well as provided the space for loading silver nanoparticles. Ag nanoparticles were fabricated and deposited onto the surface of porous Fe_3O_4@Carbon substrate with the assistance of ultrasound treatment. Studies on the catalytic properties and the antibacterial activities of the composite matrices demonstrated that the effective catalytic activity and the high antibacterial efficiency arose from the anchored Ag nanoparticles of the Ag-(Fe_3O_4@Carbon) matrices. The composite catalyst

exhibited also flexible magnetic separability due to the encapsulation of Fe_3O_4 nanoparticles. These properties revealed their potential application in biomedical field, environmental area and chemical industry with the ability of recycling by means of an external magnetic field.

Acknowledgements

This work is supported by the National Key Project on Basic Research (Grant No. 2012CB722705), the National High Technology Research and Development Program of China (Nos. 2012AA110407 and 2014AA250323) and the Natural Science Foundation of China (Nos. 21103096 and U1232104).

References:

[1] Z. Xu, Y. Hou, S.H. Sun, Magnetic Core/Shell Fe_3O_4/Au and Fe_3O_4/Au/Ag nanoparticles with tunable plasmonic properties, J. Am. Chem. Soc. 129 (2007) 8698-8699.

[2] X.Y. Yang, X.Y. Zhang, Y.F. Ma, Y. Huang, Y.S. Wang, Y.S. Chen, Superparamagnetic graphene oxide–Fe_3O_4 nanoparticles hybrid for controlled targeted drug carriers, J. Mater. Chem. 19 (2009) 2710-2714.

[3] C.T. Chen, Y.C. Chen, Fe_3O_4/TiO_2 core/shell nanoparticles as affinity probes for the analysis of phosphopeptides using TiO_2 surface-assisted laser desorption/ionization mass spectrometry, Anal. Chem. 77 (18) (2005) 5912-5919.

[4] Y. Ling, J. Luo, Q. Fan, M. Suzuki, I.S. Suzuki, M.H. Engelhard, Y.H. Lin, N. Kim, J.Q. Wang, C.J. Zhong, Monodispersed Core−Shell Fe_3O_4@Au Nanoparticles, J. Phys. Chem. B 109 (46) (2005) 21593-21601.

[5] J.F. Liu, Z.S. Zhao, G.B. Jiang, Coating Fe_3O_4 magnetic nanoparticles with humic acid for high efficient removal of heavy metals in water, Environ. Sci. Technol. 42 (18) (2008) 6949-6954.

[6] H.H. Yang, S.Q. Zhang, X.L. Chen, Z.X. Zhuang, J.G. Xu, X.R. Wang, Magnetite-containing spherical silica nanoparticles for biocatalysis and bioseparations, Anal. Chem. 76 (2004) 1316-1321.

[7] H.L. Li, J.J. Sang, J.H. Zhao, A.P. Fu, H. Liu, M. Xu, G.S. Pang, X.S. Zhao, Preparation of magnetically separable mesoporous Co@carbon/silica composites by the RAPET method, New J. Chem. 36 (2012) 2308-2315.

[8] L.M. Liz-Marzán, M. Giersig, P. Mulvaney, Synthesis of nanosized gold-silica core-shell particles, Langmuir 12 (1996) 4329-4335.

[9] H. Wang, J. Shen, Y.Y. Li, Z.Y. Wei, G.X. Cao, Z. Gai, K.L. Hong, P. Banerjee, S.Q. Zhou, Porous carbon protected magnetite and silver hybrid nanoparticles: morphological control, recyclable catalysts, and multicolor cell imaging, ACS Appl. Mater. Interfaces 5 (19) (2013) 9446-9453.

[10] S. Li, X.L. Yan, Z. Yang, Y.Z. Yang, X.G. Liu, J. Zou, Preparation and antibacterial property of silver decorated carbon microspheres, Appl. Surf. Sci. 292 (2014) 480-487

[11] V.K. Sharma, R.A. Yngard, Y. Lin, Silver nanoparticles: green synthesis and their antimicrobial activities, Adv. Colloid Interface Sci. 145 (1-2) (2009)83-96.

[12] A.M. Abdel-Mohsen, R. Hrdina, L. Burgert, R.M. Abdel-Rahman, M. Hašová, D. Šmejkalová, M. Kolář, M. Pekar, A.S. Aly, Antibacterial activity and cell viability of hyaluronan fiber with silver nanoparticles, Carbohydr. Polym. 92(2) (2013)1177-1187.

[13] L. Guo, W. Yuan, Z. Lu, C.M. Li, Polymer/nanosilver composite coatings for antibacterial applications, Colloids Surf. A- Physicochem. Eng. Asp. 439 (2013) 69-83.

[14] H.Q. Xia, B. Cui, J.H. Zhou, L.L. Zhang, J. Zhang, X.H. Guo, H.L. Guo, Synthesis and characterization of Fe_3O_4@C@Ag nanocomposites and their antibacterial performance, Appl. Surf. Sci. 257 (2011) 9397-9402.

[15] S. J. Park, Y. S. Jang, J. Preparation and characterization of activated carbon fibers supported with silver metal for antibacterial behavior, Colloid Interface Sci. 261 (2) (2003) 238-243.

[16] S.T. Zhang, D.C. Wu, L. Wan, H.B. Tan, R.W. Fu, Adsorption and antibacterial activity of silver-dispersed carbon aerogels, J. Appl. Polym. Sci. 102 (2) (2006) 1030-1037.

[17] J.D. Kim, H. Yun, G.C. Kim, C.W. Lee, H. C. Choi, Antibacterial activity and reusability of CNT-Ag and GO-Ag Nanocomposites, Appl. Surf. Sci. 283 (2013) 227-233.

[18] H.Z. Zardini, A. Amiri, M. Shanbedi, M. Maghrebi, M. Baniadam, Enhanced antibacterial activity of amino acids-functionalized multi walled carbon nanotubes by a simple method, Colloids Surf. B 92 (1) (2012) 196-202.

[19] L. Cheng, P. Guo， R. Wang, L. Ming, F. Leng, H. Li, X.S. Zhao, Electrocapacitive properties of supercapacitors based on hierarchical porous carbons from chestnut shell, Colloids Surf. A-Physicochem. Eng. Asp. 446 (2014) 127-133.

[20] S.M. Yuan, J.X. Li, L.T. Yang, L.W. Su, L. Liu, Z. Zhou, Preparation and lithium storage performances of mesoporous Fe_3O_4@C microcapsules, ACS Appl. Mater. Interfaces 3 (3) (2011) 705-709.

[21] A.H. Lu, W.C. Li, A. Kiefer, W. Schmidt, E. Bill, G. Fink, F. Schuth, Fabrication of magnetically separable mesostructured silica with an open pore system, J. Am. Chem. Soc. 126 (2004) 8616-8617.

[22] M.L. Pang, J.Y. Hu, C. H. Zeng, Synthesis, Morphological control, and antibacterial properties of hollow solid Ag_2S/Ag heterodimers, J. Am. Chem. Soc. 132 (2010) 10771-10785.

[23] R. Buonsanti, V. Grillo, E. Carlino, C. Giannini, F. Gozzo, M. Garcia-Hernandez, M.A. Garcia, R.Cingolani, P.D. Cozzoli, Architectural control of seeded-grown magnetic-semiconductor iron oxide-TiO_2 nanorod heterostructures: The role of seeds in topology selection, J. Am. Chem. Soc. 132 (2010) 2437-2464.

[24] Y. Zhan, F. Meng, X. Yang, X. Liu, Magnetite-graphene nanosheets (GNs)/poly(arylene ether nitrile) (PEN): Fabrication and characterization of a multifunctional nanocomposite film, Colloids Surf. A: Physicochem. Eng. Asp. 390 (2011) 112-119.

[25] Z. Teng, X. Su, G. Chen, C. Tian, H. Li, L. Ai, G. Lu, Superparamagnetic high-magnetization composite microspheres with Fe_3O_4@SiO_2 core and highly crystallized mesoporous TiO_2 shell, Colloids Surf. A: Physicochem. Eng. Asp. 402 (2012) 60-65.

[26] N. Linares, E. Serrano, M. Rico, A.M. Balu, E. Losada, R. Luque, J. García-Martínez, Incorporation of chemical functionalities in the framework of mesoporous silica, Chem. Commun. 47 (2011) 9024-9035.

[27] A. Popat, S.B. Hartono, F. Stahr, J. Liu, S.Z. Qiao, G.Q. Lu, Mesoporous silica nanoparticles for bioadsorption, enzyme immobilisation, and delivery carriers, Nanoscale, 3 (7) (2011) 2801-2818.

[28] Y. Deng, Y. Cai, Z. Sun, D. Zhao, Magnetically responsive ordered mesoporous materials: a burgeoning family of functional composite nanomaterials, Chem. Phys. Lett. 510 (1) (2011) 1-13.

[29] Y. Deng, D. Qi, C. Deng, X. Zhang, D. Zhao, Superparamagnetic high-magnetization microspheres with an Fe_3O_4@SiO_2 core and perpendicularly aligned mesoporous SiO_2 shell for removal of microcystins, J. Am. Chem. Soc. 130(1) (2008) 28-29.

[30] M. Liong, S. Angelos, E. Choi, K. Patel, J.F. Stoddart, J.I. Zink, Mesostructured multifunctional nanoparticles for imaging and drug delivery, J. Mater. Chem. 19 (2009) 6251-6257.

[31] S. Liu, R. Xing, F. Lu, R.K. Rana, J.J. Zhu, One-pot template-free fabrication of hollow magnetite nanospheres and their application as potential drug carriers, J. Phys. Chem. C 113 (50) (2009) 21042-21047.

[32] M. Xia, C. Chen, M. Long, C. Chen, W. Cai, B. Zhou, Magnetically separable mesoporous silica nanocomposite and its application in Fenton catalysis, Microp. Mesop. Mater. 145 (2011) 217-223.

[33] W. L. Shi, H. Zeng, Y. Sahoo, T.Y. Ohulchanskyy, Y. Ding, Z. L. Wang, M. Swihart, P. N. Prasad, A general approach to binary and ternary hybrid nanocrystals, Nano Lett. 6 (2006) 875-881.

[34] D. Wang, Y. Li, One-pot protocol for Au-based hybrid magnetic nanostructures via a noble-metal-induced reduction process, J. Am. Chem. Soc. 132 (2010) 6280-6281.

[35] Y. Pan, J. Gao, B. Zhang, X. Zhang, B. Xu, Colloidosome-based synthesis of a multifunctional nanostructure of silver and hollow iron oxide nanoparticles， Langmuir 26 (2009) 4184-4187.

[36] H. Deng, X.L. Li, Q. Peng, X. Wang, J.P. Chen, Y.D. Li, Monodisperse magnetic single-crystal ferrite microspheres, Angew. Chem. Int. Edit. 44 (2005) 2782-2785.

[37] O. Akhavan, Lasting antibacterial activities of Ag–TiO_2/Ag/a-TiO_2 nanocomposite thin film photocatalysts under solar light irradiation, J. Colloid Interf. Sci. 336 (2009) 117-124.

[38] K. Xu, J. X. Wang, X. L. Kang, Fabrication of antibacterial monodispersed Ag–SiO_2 core–shell nanoparticles with high concentration, J. F. Chen, Mater. Lett. 63 (2009) 31-33.

[39] J. M. Qu, G. Liu, Y. M. Wang, R. Y. Hong, Preparation of Fe_3O_4–chitosan nanoparticles used for hyperthermia, Adv. Powder Technol. 21 (2010) 461-467.

[40] J. Serra, P. González, S. Liste,S. Chiussi, B. León, M. Pérez-Amor, H.O.Ylänen, M. Hupa, Influence of the non-bridging oxygen groups on the bioactivity of silicate glasses, J. Mater. Sci. Mater. Med. 13 (2002) 1221-1225.

[41] Q.L. Li, H.L. Li, V. Pol, I. Bruckental, Y. Koltypin, J. Calderon-Moreno, I. Nowik, A. Gedanken, Sonochemical synthesis, structural and magnetic properties of air-stable Fe/Co alloy nanoparticles, New J. Chem. 27 (2003) 1194-1199.

[42] H.L. Li, R.Z. Wang, H. Qi, Z.Y. Zhong, K. Yuri, J. Calderon-Moreno, A. Gedanken, Ultrasound-assisted polyol method for the preparation of sba-15-supported ruthenium nanoparticles and the study of their catalytic activity on the partial oxidation of methane, Langmuir, 19 (2004) 8352-8356.

[43] V. G. Pol, D.N. Srivastava, O. Palchik, V. Palchik, M.A. Slifkin, A.M. Weiss, A. Gedanken, Sonochemical deposition of silver nanoparticles on silica spheres, Langmuir 18 (2002) 3352-3357.

[44] S. Chen, H. Zeng, Improvement of the reduction capacity of activated carbon fiber, Carbon 41(2003) 1265-1271.

[45] R.R. Xu, W.Q. Pang, J.H. Yu, J.S. Chen, Chemistry of Zeolites and Related Porous Materials: Synthesis and Structure, Wiley, (2009) 146-147.

[46] H. Liu, H.L. Li, Z.L. Ding, H.Y. Wang, P.Z. Guo, J.Q. Yu, C.G. Wang, X.S. Zhao, Preparation of Porous Hollow SiO2 Spheres by a Modified Stöber Process Using MF Microspheres as Templates, J. Clust. Sci. 23 (2012) 273-285.

[47] G. James, P. Pankaj, A. James, S. Sanyadanam, S. Hariharan, Superparamagnetic polymer nanocomposites with uniform Fe_3O_4 nanoparticle dispersions, Adv. Funct. Mater. 16 (2006) 71-75.

[48] K. Woo, J.W Hong, S. Choi, H.W. Lee, J.P. Ahn, C.S. Kim, and S.W. Lee, Easy synthesis and magnetic properties of iron oxide nanoparticles, Chem. Mater. 16 (2004) 2814-2818.

[49] Y.H. Deng, Y. Cai, Z.K. Sun, J. Liu, C. Liu, J. Wei, W. Li, C. Liu, Y. Wang, D.Y. Zhao, Multifunctional mesoporous composite microspheres with well-designed nanostructure: a highly integrated catalyst system, J. Am. Chem. Soc. 132 (24) (2010) 8466–8473.

[50] N. Pradhan, A. Pal, T. Pal, Silver nanoparticle catalyzed reduction of aromatic nitro compounds, Colloid. Surface. A 196 (2) (2002) 247-257.

[51] S. Jana, S.K. Ghosh, S. Nath, S. Pande, S. Praharaj, S. Panigrahi, S. Basu, T. Endo, T. Pai, Synthesis of silver nanoshell-coated cationic polystyrene beads: A solid phase catalyst for the reduction of 4-nitrophenol, Appl. Catal. A-Gen. 313 (1) (2006) 41-48.

[52] Y.H. Zhu, J.H. Shen, K.F. Zhou, C. Chen, X.L. Yang, C.Z. Li, Multifunctional magnetic composite microspheres with in situ growth Au nanoparticles: a highly efficient catalyst system, J. Phys. Chem. C 115 (5) (2011) 1614–1619.

[53] N. Pradhan, A. Pal, T. Pal, Catalytic reduction of aromatic nitro compounds by coinage metal nanoparticles, Langmuir 17 (5) (2001) 1800-1802.

[54] B. Naik, S. Hazra, V.S. Prasad, N.N. Ghosh, Synthesis of Ag nanoparticles within the pores of SBA-15: An efficient catalyst for reduction of 4-nitrophenol, Catal. Commun. 12 (12) (2011) 1104-1108.

[55] H.J. Jeon, S.C. Yi, Preparation and antibacterial effects of Ag–SiO_2 thin films by sol–gel method, Biomaterials 24 (27) (2003) 4921-4928.

[56] C. Marambio-Jones, E.M.V. Hoek, A review of the antibacterial effects of silver nanomaterials and potential implications for human health and the environment, J. Nanopart. Res. 12 (2010) 1531-1551.

Scheme and Figure captions

Scheme 1. Formation process of the porous Fe_3O_4@Carbon composite particles (FC).

Fig. 1 FT-IR spectra of (A) Fe_3O_4, (B) (SiO_2, Fe_3O_4)@Chitosan, (C) (SiO_2, Fe_3O_4)@Carbon, and (D) porous Fe_3O_4@Carbon.

Fig. 2 SEM images of (A) Fe_3O_4 microspheres, (B) FC-1, (C) FC-2 and (D) FC-3.

Fig. 3 TEM images of (A) FC-3, (B) Ag-FC-U and (C) Ag-FC-M.

Fig. 4 XRD patterns of the Fe_3O_4 nanoparticles (curve A), the porous Fe_3O_4@Carbon particles (curve B), and those of the Ag nanoparticles decorated Fe_3O_4@Carbon composite particles (curve C, Ag-FC-U and curve D, Ag-FC-M).

Fig. 5 Nitrogen adsorption-desorption isotherms and the corresponding pore-size distributions (the inset) of FC-3 and Ag-FC-U.

Fig. 6 Room-temperature magnetic hysteresis loops of (A) Fe_3O_4, (B) Fe_3O_4@Carbon, (C) Ag-(Fe_3O_4@Carbon). The bottom inset is a magnification of the magnetic hysteresis loops. The upper inset is a photograph of the adsorption of MB by Ag-(Fe_3O_4@Carbon) and their response to an external magnet.

Fig. 7 UV-Vis spectra of 4-NP in the absence or presence of $NaBH_4$ (a); Time dependent UV-Vis spectra for the catalytic reduction of 4-NP using Ag-(Fe_3O_4@Carbon) (Ag-FC-U) as a catalyst (b); and Photographs of the reduction of 4-NP by $NaBH_4$ in the presence of Ag-(Fe_3O_4@Carbon) and the magnetic separation of the catalyst after the catalytic reaction (c).

Fig. 8 Photographs of the antibacterial test results for FC-3 (A, C) and Ag-FC-U (B, D) against E. coli (A, B) and S. aureus (C, D).

Fig. 9 Photographs of the tubes used for determining the minimum inhibitory concentrations of Ag-FC-U composites against E. coli (left) and S. aureus (right).